ADVANCED FUNCTIONAL MATERIALS
www.afm-journal.de

www.MaterialsViews.com

General Formation of MS (M = Ni, Cu, Mn) Box-in-Box Hollow Structures with Enhanced Pseudocapacitive Properties

*Xin-Yao Yu, Le Yu, Laifa Shen, Xiaohui Song, Hongyu Chen, and Xiong Wen (David) Lou**

Complex hollow structures of metal sulfides could be promising materials for energy storage devices such as supercapacitors and lithium-ion batteries. However, it is still a great challenge to fabricate well-defined metal sulfides hollow structures with multi-shells, hierarchical architectures, and non-spherical shape. In this work, a template-engaged strategy is developed to synthesize hierarchical NiS box-in-box hollow structures with double-shells. The NiS box-in-box hollow structures constructed by ultrathin nanosheets are evaluated as electrode materials for supercapacitors. As expected, the NiS box-in-box hollow structures exhibit excellent rate performance and impressive cycling stability due to their unique nano-architecture. More importantly, the synthetic method can be easily extended to synthesize other transition metal sulfides box-in-box hollow structures. For example, we have also successfully synthesized similar CuS and MnS box-in-box hollow structures. The present work makes a significant contribution to the design and synthesis of transition metal sulfides hollow structures with non-spherical shape and complex architecture, as well as their potential applications in electrochemical energy storage.

1. Introduction

Hollow micro-/nanostructures, especially those with complex multi-shelled structures, are attracting fast growing interest due to their potential applications in many fields, such as gas sensors, catalysis, energy conversion, and storage systems.[1–5] Recently, numerous synthetic strategies have been proposed to create complex multi-shelled hollow structures that exhibit superior performance to their conventional simple single-shelled counterparts in many applications.[6–10] Among the available synthetic methodologies, hard-templating methods have been demonstrated most versatile to generate well-defined complex hollow structures with controlled shell number and high uniformity.[2,8,11,12] For example, Wang and co-workers reported the synthesis of multi-shelled SnO_2 hollow spheres for high-performance dye-sensitized solar cells by using alkali-treated carbonaceous microspheres as templates.[12] Xie et al. reported the synthesis of multi-shelled VOOH hollow spheres using $V(OH)_2NH_2$ solid spheres as the self-template via a programmed reaction process.[13] We have recently developed a new "penetration-solidification-annealing" strategy to synthesize various mixed metal oxide multi-shelled hollow spheres using carbon nanospheres as hard templates.[11] It is found that these multi-shelled hollow spheres possess remarkable electrochemical properties for reversible lithium storage.

Notwithstanding the above-mentioned advances, in most cases, the resulting hollow structures are spherical in shape. Synthesis of hollow particles with well-defined non-spherical shapes and multi-shells thus remains a significant challenge. This could be largely ascribed to the deficiency of non-spherical templates and difficulty in forming uniform coatings, especially multi-layered coatings around high-curvature surfaces.[5,6] On the other hand, present research mostly focuses on nanostructured metal oxides, while hollow metal sulfides with complex multi-shelled structures are still scarcely reported. Therefore, it is highly desirable yet challenging to develop novel synthetic systems to fabricate high-quality complex non-spherical metal sulfide hollow particles.

Nanostructured metal sulfides with unique physical and chemical properties as well as high specific capacitance or capacity have emerged as prominent electrode materials for supercapacitors (SCs) and lithium-ion batteries (LIBs).[14–23] Transitional metal sulfides usually exhibit higher conductivity than their oxide counterparts, providing facilitated pathway for electron transport.[24,25] On the other hand, many transitional metal sulfides possess layered crystal structures. As a result, two-dimensional (2D) nanosheet structures are often formed from metal sulfides, offering a large specific surface area and interlayer space for ion intercalation.[26] Despite that great efforts have been made, the implementation of metal sulfides-based electrodes in practical applications is hindered by their low specific capacitance/capacity, poor rate performance and cycling stability. To circumvent these difficulties, nanoscale metal sulfides combined with nanostructured carbon[17,18,20] and hollow metal sulfides nanostructures[16,19,22] have been

Dr. X. Y. Yu, L. Yu, L. F. Shen, Prof. X. W. Lou
School of Chemical and Biomedical Engineering
Nanyang Technological University
62 Nanyang Drive, Singapore 637459
E-mail: xwlou@ntu.edu.sg; davidlou88@gmail.com
X. H. Song, Prof. H. Y. Chen
Division of Chemistry and Biological Chemistry
Nanyang Technological University
Singapore 637371

DOI: 10.1002/adfm.201402560

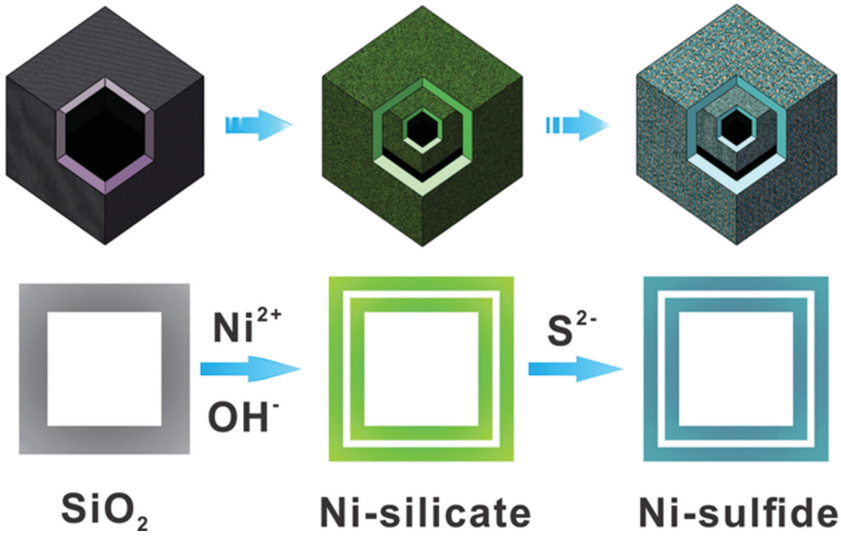

Figure 1. Schematic illustration for the formation process of the nickel sulfide box-in-box hollow structure.

developed to improve their electrochemical properties. Use of complex hollow metal sulfides with unique multi-shelled structures and hierarchical architectures is expected to be able to further improve their electrochemical performance. Hollow structures with multi-shells increase the electrode/electrolyte contact area and provide more electroactive sites, which might lead to higher specific capacitance/capacity. The nanoscale building blocks can also shorten the path of ionic and electronic transport, resulting in improved rate performance.[17,18] Furthermore, multi-shelled particles might exhibit better structural robustness and accommodate the mechanical strain and structural distortion from ion insertion or extraction and surface redox reactions during cycling, thereby contributing to good cycling performance.[11]

Herein, we report the synthesis of ultra-thin NiS nanosheets constructed box-in-box hollow structures with double shells via a novel template-engaged method. When investigated as electrode materials for SCs, the as-synthesized NiS box-in-box hollow structure manifests enhanced rate performance and good cycling stability. Moreover, this synthetic strategy can be extended as a general approach to prepare other transition metal sulfides with the box-in-box architecture.

2. Results and Discussion

The novel hierarchical NiS box-in-box hollow nanostructure is formed via a facile template-assisted method. As schematically illustrated in **Figure 1**, uniform silica nanoboxes are first prepared using Fe_2O_3 nanocubes as the template. Silica nanoboxes act as not only the template but also the starting material for the subsequent reactions. Then, nickel silicate box-in-box hollow nanostructures are synthesized through a simple hydrothermal method using silica nanoboxes as the self-sacrificial template. Silica (SiO_2) nanoboxes are dispersed into an alkaline solution containing nickel acetate, ammonia, and ammonium chloride. Ammonia can generate an alkaline environment and also form complex ions with Ni^{2+}. Ammonium chloride is used to control the ionization rate of ammonia and restrain the formation of nickel hydroxide by introduction of additional ammonium ions.[28] In the initial stage of the hydrothermal process, SiO_2 is partially dissolved to form silicate anions under the alkaline condition at high temperature, which react with Ni^{2+} to form a thin layer of nickel silicate and preferentially deposit on the surface of silica nanoboxes.[29–32] As the reaction proceeds, the SiO_2 core continuously dissolves and releases silicate anions, which diffuse outwards and supply the growth of preformed nickel silicate shell. A gap is thus formed between the remaining SiO_2 core and the nickel silicate shell. When the gap enlarges to a certain degree, the generated silicate anions would react with inward diffused Ni^{2+} before they reach with the outer shell. As a result, a secondary nickel silicate shell is generated on the surface of the remaining SiO_2 core. Upon the completion of reaction, a double-shelled box-in-box nickel silicate hollow structure is eventually produced. In the final step, the as-prepared box-in-box nickel silicate structure is converted into nickel sulfide box-in-box hollow nanostructures through a solution-based sulfidation method in the presence of Na_2S.

The initial cubic Fe_2O_3 particles are prepared by a simple co-precipitation method.[27] Powder X-ray diffraction (XRD) measurement confirms the successful synthesis of Fe_2O_3 templates (Figure S1, see Supporting Information). **Figure 2**a shows the field-emission scanning electron microscope (FESEM) image of Fe_2O_3 nanocubes, indicating that the cubic Fe_2O_3 particles are highly uniform with a size about 500 nm. Core–shell structured Fe_2O_3@silica particles are obtained by a modified Stöber's method (Figure S2a, see Supporting Information). After removing the core templates by hydrochloric acid etching, the cubic silica shell structure is well maintained (Figure S2b, see Supporting Information). Figure 2b,c gives typical transmission electron microscopy (TEM) images of the silica nanoboxes. A well-defined pseudo-cubic void is clearly observed by the sharp contrast between the center and the edge, and the thickness of the shell is determined to be about 100 nm. In addition, the surface of SiO_2 nanoboxes is relatively smooth due to its amorphous character (Figure 2c). After hydrothermal treatment in alkaline solution containing nickel ions at 100 °C for 12 h, the as-obtained samples retain the cubic morphology, while the surface becomes much rougher (Figure 2d). The crystallographic structure and phase purity of the nickel silicate box-in-box nanostructures are examined by XRD. All the major peaks of the XRD pattern (Figure S3, see Supporting Information) can be clearly indexed to nickel silicate ($Ni_3Si_4O_{10}(OH)_2 \cdot 5H_2O$, JCPDS card No. 43–0664). The apparent broadening of these peaks indicates that the as-prepared nickel silicate is composed of nanoscale crystallites. The box-in-box architecture of the obtained nickel silicate particles can be verified through both FESEM and TEM observations, as shown in Figure 2e–g. From a cracked particle shown in Figure 2e, the inner shell can be

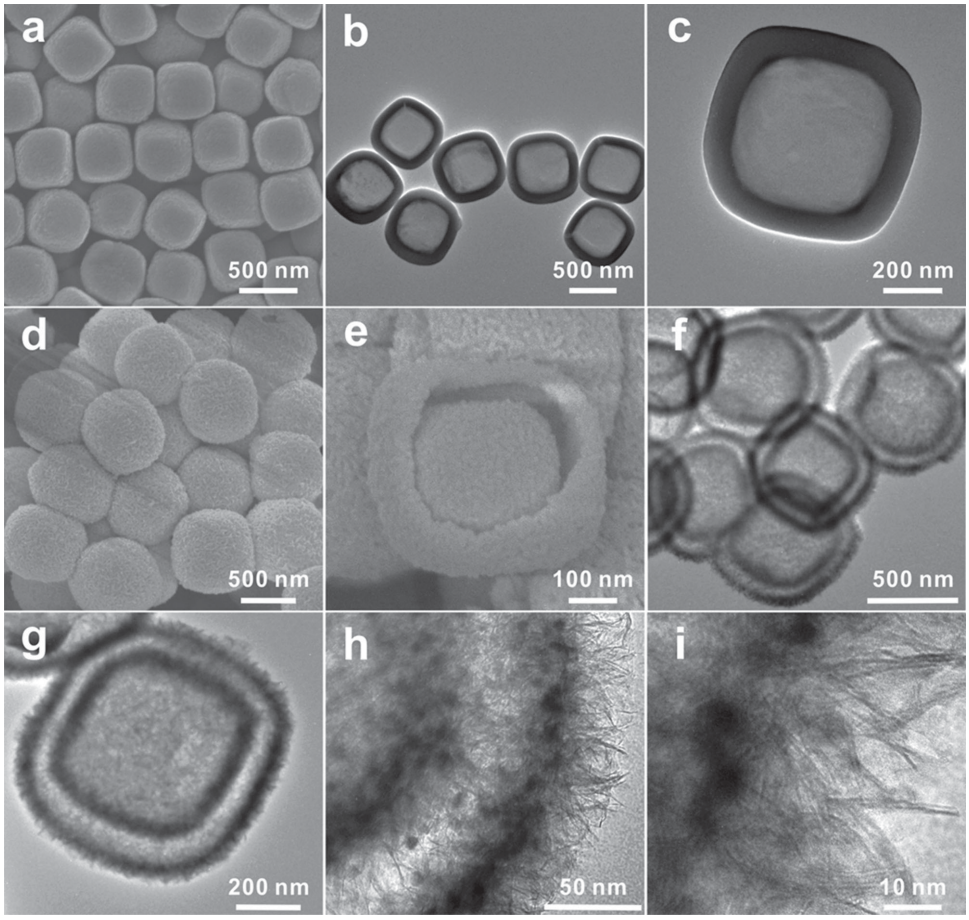

Figure 2. a,d,e) FESEM and b,c,f–i) TEM images of Fe_2O_3 nanocubes (a), SiO_2 nanoboxes (b,c), and nickel silicate box-in-box hollow structures (d–i).

clearly observed with a similar morphological feature as that of the outer shell, both of which are constructed by ultrathin nanosheets (Figure 2d). TEM observation (Figure 2f,g) indicates that the as-synthesized nickel silicates possess a unique box-in-box hollow structure, in which an obvious gap between the outer and inner shells can be clearly observed. Estimated from the enlarged TEM image shown in Figure 2g, the thickness of the outer shell is nearly identical to that of the inner shell, with an average thickness of around 50 nm. The enlarged view of the nickel silicate box-in-box hollow particles (Figure 2h,i) reveals that both of the shells are constructed by ultrathin and curved nanosheets with a small thickness of a few nanometers.

The nickel silicate box-in-box hollow structure is chemically converted to nickel sulfide under hydrothermal conditions by reacting with Na_2S. **Figure 3**a shows the XRD pattern of the as-synthesized sample after sulfidation. All the peaks can be readily indexed to the rhombohedral NiS phase (JCPDS card No. 86–2281)[33] by comparing with the standard pattern, indicating the complete sulfidation of nickel silicate. The morphology and structure of the NiS sample are characterized by FESEM and TEM observation (Figure 3b–f). Figure 3b–d show some representative FESEM and TEM images of NiS. Obviously, the NiS sample completely maintains the box-in-box hollow structure of nickel silicate without noticeable variation. A close examination of the sample reveals that the thickness of shells is kept almost unchanged (Figure 3e). A magnified TEM image shown in Figure 3f clearly reveals that the shell of NiS is also composed of ultrathin nanosheets well preserved from the nickel silicate nanosheets, despite the slightly reduced size. In virtue of the hollow structure and the ultrathin nanosheets, the as-prepared hierarchical NiS box-in-box hollow structure possesses a relatively high Brunauer-Emmett-Teller (BET) surface area of 140.28 $m^2\ g^{-1}$ and a high pore volume of 0.3 $cm^3\ g^{-1}$, with pore sizes mostly below 10 nm (nitrogen adsorption-desorption isotherms are given in Figure S4, see Supporting Information).

To demonstrate the potential application of such novel complex hollow structure, the NiS box-in-box hollow particles are evaluated as electrode materials for SCs. **Figure 4**a shows representative cyclic voltammetry (CV) curves of the electrode in a voltage window of 0.15 to 0.55 V versus a standard calomel electrode (SCE) with various sweeping rates. Apparently, the shape of CV curves is distinct from that of electric double-layer capacitance, demonstrating pronounced pseudocapacitive characteristics. A pair of well-defined redox peaks related to Faradaic reaction can be observed at around 0.36/0.47 V (cathodic/anodic) at a low sweep rate, which corresponds to the reversible conversion between Ni(II) and Ni(III).[14] It can be seen that all of the redox peaks are symmetrical with different scan rates, which is an indication of the excellent reversibility of the redox

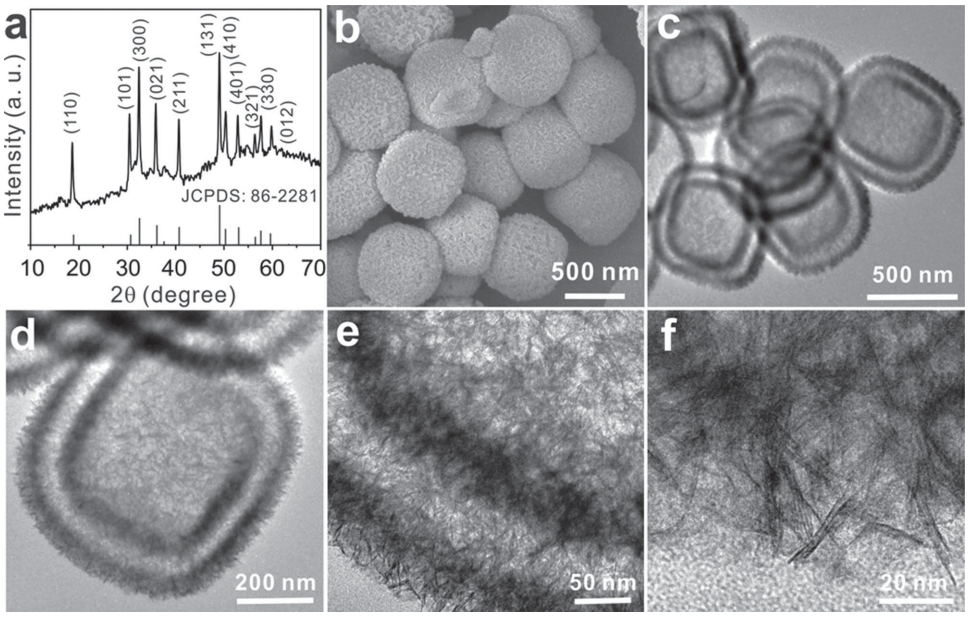

Figure 3. a) XRD pattern, b) FESEM, and c–f) TEM images of NiS box-in-box hollow structures.

reaction at/near the surface of NiS material. In addition, with an increasing scan rate, the shape of the curves is maintained, implying the excellent rate performance of the electrode.

Figure 4b shows the galvanostatic charge/discharge measurements performed in a voltage range between 0 and 0.5 V (vs SCE) at various current densities from 1 to 20 A g^{-1}. As can be seen, the potential plateaus in the charge–discharge curves are in good agreement with the results of the CV measurements. The specific capacitance is calculated by the formula, $C = I\Delta t/m\Delta V$, where I is the discharge current, Δt is the discharge time, ΔV is the voltage range and m is the mass of the electroactive materials. The current-density dependence of

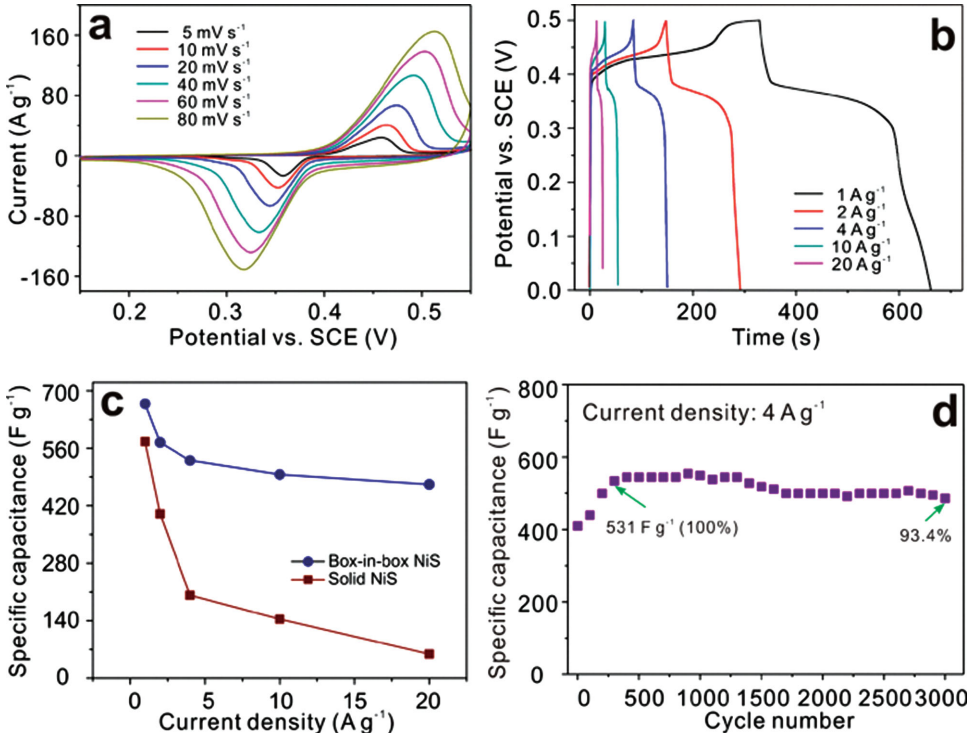

Figure 4. Electrochemical characterizations of the NiS box-in-box hollow structure: a) CV curves at different scan rates. b) Charge–discharge curves at different current densities, and c) the corresponding specific capacitance calculated from the discharge curves. d) Cycling performance at a constant current density of 4 A g^{-1}. For comparison purpose, rate capability of NiS solid particles is also included in (c).

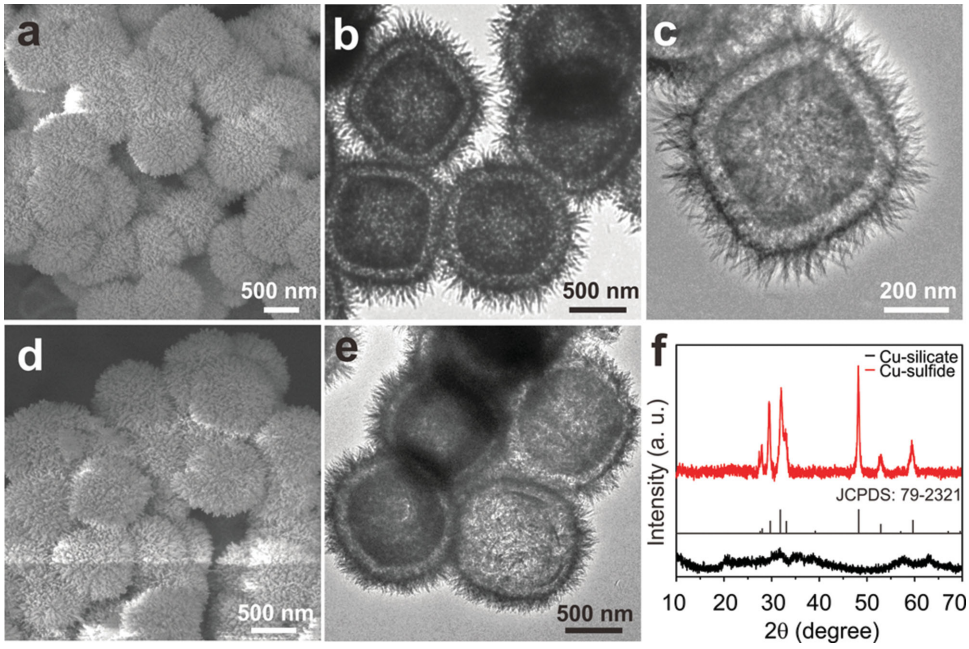

Figure 5. a,d) FESEM and b,c,e) TEM images of copper silicate (a–c) and copper sulfide box-in-box hollow structures (d,e). f) XRD patterns of copper silicate and copper sulfide.

specific capacitance is calculated from galvonostatic charge/discharge curves and depicted in Figure 4c. The NiS box-in-box hollow structure can deliver a high specific capacitance of 668 F g^{-1} at a current density of 1 A g^{-1}. More importantly, at a high current density of 20 A g^{-1}, the specific capacitance of the electrode remains at 472 F g^{-1}, which is 71% of the value obtained at 1 A g^{-1}, highlighting the excellent rate capability of the NiS box-in-box hollow structure.

Figure 4d shows cycling stability of the NiS box-in-box hollow structure with a plot of specific capacitance as a function of cycling number at a current density of 4 A g^{-1}. Interestingly, during the initial 400 cycles, the specific capacitance gradually increases from 405 to 531 F g^{-1}. It is believed that an activation process occurs during the initial 400 cycles.[34,35] After that, the electrode is fully activated and reaches a maximal capacitance, and tends to stabilize afterwards. Impressively, after the subsequent 2600 continuous charge–discharge cycles, 93.4% of the maximal capacitance is still retained, exhibiting good cycling stability. The supercapacitive performance of these NiS box-in-box hollow structures is superior to that of solid nickel sulfides in terms of rate capability and cycling performance (Figue 4c, and Figure S5 in Supporting Information). Such desirable pseudocapacitive performance of the NiS box-in-box hollow structure might be attributed to their unique structural features. Specifically, the ultrathin nanosheets building blocks ensure the facile diffusion of the electrolyte ion and endow more active sites for electrochemical reactions, thus resulting in the high electrochemical activity.[17] The empty space could serve as a reservoir for electrolyte, hence benefiting a good rate capability.[16,34] Moreover, the unique double-shelled structure with high specific surface area provides more contact area between electrode materials and electrolyte, maximizing the utilization of the hollow structure and realizing a high pseudocapacitance.[24,36,37] More importantly, the novel box-in-box hollow architecture could improve the structural integrity during cycling, which might largely contribute to the excellent cycling stability.[36,37]

Importantly, this template-assisted method is rather general and can be also used to prepare box-in-box hollow structures with different functional building blocks such as copper silicates and manganese silicates and their derived metal sulfides. **Figure 5**a–e and **Figure 6**a–e show typical FESEM and TEM images of copper silicate/sulfide and manganese silicate/sulfide, respectively. As can be seen, similar metal silicate box-in-box hollow structures can be synthesized using a similar method. It is observed that there is some important difference in the building units of the shells. The double shells of CuS box-in-box hollow structures are constructed by ultrafine nanoneedles, whereas the primary building blocks of the double shells of MnS box-in-box hollow structures are nanoparticles. After sulfidation, CuS and MnS can be obtained with well-maintained morphology and well-defined double-shelled box-in-box structures. Their corresponding XRD patterns (Figure 5f, 6f) can all be well indexed to the respective phases without any impurity peaks. These interesting hollow structures with double shells and unique building blocks may have potential applications in many important areas such as solar cells, electrocatalysts, SCs and LIBs. Although all of the hollow structures in this study exclusively show double shells, our preliminary results show that it would be possible to tune the number of shells by precisely controlling the experimental conditions, such as the shell thickness of silica nanoboxes and the initial concentration of metal ions. It is also possible to extend this strategy to make complex hollow structures of other shapes, for example, tubular structures. This versatile and controllable synthesis method would provide a venue to fully optimize the structure and performance of complex hollow structures.

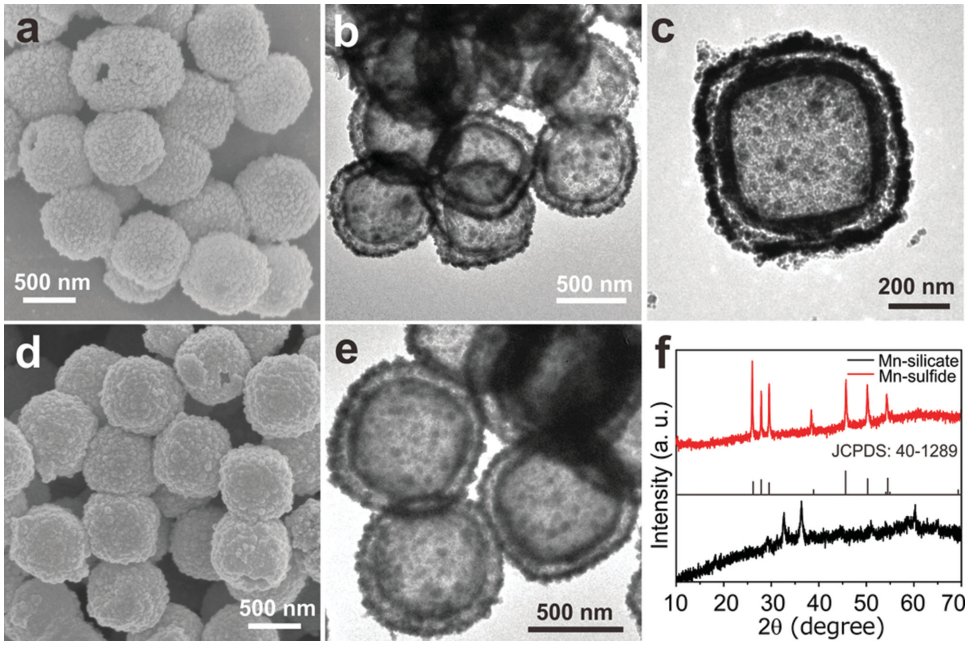

Figure 6. a,d) FESEM and b,c,e) TEM images of manganese silicate (a-c) and manganese sulfide box-in-box hollow structures (d,e). f) XRD patterns of manganese silicate and manganese sulfide.

3. Conclusions

In summary, we have successfully developed a facial template-assisted method for synthesis of unique hierarchical box-in-box hollow structures of metal sulfides. This method first involves the synthesis of metal silicate box-in-box hollow structures by a simple hydrothermal method. Then, the metal silicate can be converted to respective sulfides without changing the morphology by a simple sulfidation reaction. As an example, the NiS box-in-box hollow structures are further evaluated as an electrode material for supercapacitors with enhanced electrochemical performance. Specifically, these NiS box-in-box hollow structures exhibit a high specific capacitance of 668 F g^{-1} at a current density of 1 A g^{-1}, excellent rate capability (71% capacitance retention at 20 A g^{-1}), and good cycling stability (retention of 93.4% after 3000 cycles at 4 A g^{-1}). We believe that the present strategy could be applicable for the facile synthesis of novel metal sulfides hollow structures with multi-shelled architecture and great promise for various applications.

4. Experimental Section

Synthesis of Fe_2O_3 Nanocubes: Fe_2O_3 nanocubes were synthesized according to a previously reported method.[27] Typically, 50 mL of 5.4 M NaOH solution was added to the same volume of 2 M $FeCl_3$ solution during a period of 5 min under agitation at 75 °C. The resulting $Fe(OH)_3$ gel was continuously agitated at the same temperature for 5 min, and aged at 100 °C in a preheated oven for 4 days. After the reaction, the red products were collected by filtration and washed three times with deionized water and ethanol before drying at 70 °C overnight.

Synthesis of SiO_2 Nanoboxes: Synthesis of silica nanoboxes was achieved by a solution process using the prefabricated Fe_2O_3 nanocubes as a sacrificial template. Silica-coated Fe_2O_3 nanocubes were firstly prepared by a modified Stöber method. In a typical synthesis, 0.15 g of Fe_2O_3 nanocubes was dispersed in 650 mL of ethanol and 65 mL of H_2O through ultrasonication, followed by the addition of 60 mL of ammonia solution (28%). 0.5 mL tetraethylorthosilicate dissolved in 4.5 mL of absolute ethanol was slowly added into the mixture at a rate of 1 mL min^{-1} under magnetic stirring. The reaction was continued for 18–22 h before the product was collected via centrifugation, followed by washing and drying at 70 °C overnight. The as-prepared Fe_2O_3@silica core@shell nanocubes were etched with 4 M HCl solution at 100 °C for 48 h to obtain silica nanoboxes.

Synthesis of Nickel Silicate Box-in-Box Hollow Structures: The box-in-box nickel silicate hollow structures were prepared through a simple hydrothermal process. 20 mg of silica nanoboxes was first dispersed in 20 mL of deionized water through ultrasonication, and then 0.2 mmol of $Ni(CH_3COO)_2{\cdot}4H_2O$, 4 mmol of NH_4Cl, and 0.4 mL of ammonia solution (28%) were added to the above mixture under stirring. The mixture was transferred into a Teflon-lined autoclave and maintained at 100 °C for 12 h. After the autoclave was cooled down to room temperature naturally, the resulting light-green product was collected via centrifugation and washed three times with deionized water and ethanol, respectively, and dried at 70 °C overnight. The box-in-box copper silicate and manganese silicate were synthesized using a similar experimental process with slightly different amount of corresponding metal acetate, heating temperature and duration (Cu: 0.25 mmol and 140 °C for 10 h; Mn: 0.16 mmol and 140 °C for 10 h).

Synthesis of Nickel Sulfide Box-in-Box Hollow Structures: To obtain box-in-box nickel sulfide, the as-prepared nickel silicate (around 20 mg) and 50 mg of PVP (K-30) were dispersed into 30 mL of deionized water by ultrasonication for 20 min. After adding 100 mg of Na_2S, the mixture was transferred into a Teflon-lined autoclave and heated at 160 °C for 12 h. For the synthesis of box-in-box copper sulfide, the as-prepared copper silicate (around 20 mg) and 50 mg of PVP (K-30) were dispersed into 10 mL of ethanol and 20 mL of deionized water by ultrasonication for 20 min. After adding 80 mg of Na_2S, the mixture was transferred into a Teflon-lined autoclave and heated at 120 °C for 12 h. For the synthesis of manganese sulfide box-in-box structures, the as-prepared manganese silicate (around 30 mg) and 100 mg of PVP (K-30) were dispersed into 10 mL of ethanol and 20 mL of deionized water by ultrasonication for 20 min. After adding 150 mg of Na_2S, the mixture was transferred into a Teflon-lined autoclave and heated at 180 °C for 12 h. Solid NiS particles

with similar size were also prepared for comparison. Typically, 2 mmol of $NiSO_4 \cdot 6H_2O$ and 4 mmol of thiourea were dissolved in a 45 mL mixed solution of deionized water and ethylene glycol with a volume ratio of 2:1. The mixture was then transferred into a Teflon-lined autoclave and heated at 180 °C for 12 h. The products were washed thoroughly with deionized water and ethanol, and then dried at 70 °C overnight for further characterizations.

Materials Characterization: Field-emission scanning electron microscope (FESEM; JEOL-6700) and transmission electron microscope (TEM; JEOL, JEM-2010) were used to characterize the microscopic features of the samples. A Bruker D2 Phaser X-ray Diffractometer with Ni filtered Cu Kα radiation (λ = 1.5406 Å) at a voltage of 30 kV and a current of 10 mA was used to collect the XRD patterns of the products. The nitrogen sorption measurement was carried out on Autosorb 6B at liquid-nitrogen temperature.

Electrochemical Measurements: The working electrode was composed of active material, carbon black (Super-P-Li), and polymer binder (polyvinylidene fluoride, PVDF) at a weight ratio of 70:20:10. This mixture was then pressed onto Ni foam and dried at 70 °C under vacuum for 12 h. The mass loading of electroactive materials is around 1.0 mg cm^{-2}. The electrochemical tests were conducted with a CHI 660D electrochemical workstation in an aqueous KOH electrolyte (3.0 M) using a three-electrode cell with Pt foil serving as the counter electrode and a standard calomel electrode (SCE) as the reference electrode.

Supporting Information

Supporting Information is available from the Wiley Online Library or from the author.

Received: July 30, 2014
Revised: August 26, 2014
Published online: September 22, 2014

[1] M. H. Oh, T. Yu, S. H. Yu, B. Lim, K. T. Ko, M. G. Willinger, D. H. Seo, B. H. Kim, M. G. Cho, J. H. Park, K. Kang, Y. E. Sung, N. Pinna, T. Hyeon, *Science* **2013**, *340*, 964.
[2] X. Y. Lai, J. E. Halpert, D. Wang, *Energy Environ. Sci.* **2012**, *5*, 5604.
[3] X. W. Lou, L. A. Archer, Z. C. Yang, *Adv. Mater.* **2008**, *20*, 3987.
[4] J. H. Sun, J. S. Zhang, M. W. Zhang, M. Antonietti, X. Z. Fu, X. C. Wang, *Nat. Commun.* **2012**, *3*, 1339.
[5] J. B. Joo, Q. Zhang, M. Dahl, I. Lee, J. Goebl, F. Zaera, Y. D. Yin, *Energy Environ. Sci.* **2012**, *5*, 6321.
[6] G. Q. Zhang, B. Y. Xia, C. Xiao, L. Yu, X. Wang, Y. Xie, X. W. Lou, *Angew. Chem. Int. Ed.* **2013**, *52*, 8643.
[7] H. L. Xu, W. Z. Wang, *Angew. Chem. Int. Ed.* **2007**, *46*, 1489.
[8] H. G. Zhang, Q. S. Zhu, Y. Zhang, Y. Wang, L. Zhao, B. Yu, *Adv. Funct. Mater.* **2007**, *17*, 2766.
[9] Z. H. Dong, X. Y. Lai, J. E. Halpert, N. L. Yang, L. X. Yi, J. Zhai, D. Wang, Z. Y. Tang, L. Jiang, *Adv. Mater.* **2012**, *24*, 1046.
[10] J. Liu, H. Q. Yang, F. Kleitz, Z. G. Chen, T. Y. Yang, E. Strounina, G. Q. Lu, S. Z. Qiao, *Adv. Funct. Mater.* **2012**, *22*, 591.
[11] G. Zhang, X. W. Lou, *Angew. Chem. Int. Ed.* **2014**, doi/10.1002/anie.201404604.
[12] Z. H. Dong, H. Ren, C. M. Hessel, J. Y. Wang, R. B. Yu, Q. Jin, M. Yang, Z. D. Hu, Y. F. Chen, Z. Y. Tang, H. J. Zhao, D. Wang, *Adv. Mater.* **2014**, *26*, 905.
[13] C. Z. Wu, X. D. Zhang, B. Ning, J. L. Yang, Y. Xie, *Inorg. Chem.* **2009**, *48*, 6044.
[14] H. Pang, C. Z. Wei, X. X. Li, G. C. Li, Y. H. Ma, S. J. Li, J. Chen, J. S. Zhang, *Sci. Rep.* **2014**, *4*, 3577.
[15] S. W. Chou, J. Y. Lin, *J. Electrochem. Soc.* **2013**, *160*, D178.
[16] L. Yu, L. Zhang, H. B. Wu, X. W. Lou, *Angew. Chem. Int. Ed.* **2014**, *53*, 3711.
[17] T. Zhu, H. B. Wu, Y. B. Wang, R. Xu, X. W. Lou, *Adv. Energy Mater.* **2012**, *2*, 1497.
[18] T. Zhu, B. Y. Xia, L. Zhou, X. W. Lou, *J. Mater. Chem.* **2012**, *22*, 7851.
[19] T. Zhu, Z. Y. Wang, S. J. Ding, J. S. Chen, X. W. Lou, *RSC Adv.* **2011**, *1*, 397.
[20] C. S. Rout, B. H. Kim, X. Xu, J. Yang, H. Y. Jeong, D. Odkhuu, N. Park, J. Cho, H. S. Shin, *J. Am. Chem. Soc.* **2013**, *135*, 8720.
[21] Y. P. Du, Z. Y. Yin, J. X. Zhu, X. Huang, X. J. Wu, Z. Y. Zeng, Q. Y. Yan, H. Zhang, *Nat. Commun.* **2012**, *3*, 1177.
[22] J. Xia, G. C. Li, Y. C. Mao, Y. Y. Li, P. K. Shen, L. P. Chen, *CrystEngComm* **2012**, *14*, 4279.
[23] L. Zhang, L. Zhou, H. B. Wu, R. Xu, X. W. Lou, *Angew. Chem. Int. Ed.* **2012**, *51*, 7267.
[24] H. C. Chen, J. J. Jiang, L. Zhang, D. D. Xia, Y. D. Zhao, D. Q. Guo, T. Qi, H. Z. Wan, *J. Power Sources* **2014**, *254*, 249.
[25] J. W. Xiao, L. Wan, S. H. Yang, F. Xiao, S. Wang, *Nano Lett.* **2014**, *14*, 831.
[26] X. Huang, Z. Y. Zeng, H. Zhang, *Chem. Soc. Rev.* **2013**, *42*, 1934.
[27] T. Sugimoto, Y. S. Wang, H. Itoh, A. Muramatsu, *Colloids Surf., A* **1998**, *134*, 265.
[28] Y. Q. Wang, G. Z. Wang, H. Q. Wang, C. H. Liang, W. P. Cai, L. D. Zhang, *Chem. Eur. J.* **2010**, *16*, 3497.
[29] P. Jin, Q. W. Chen, L. Q. Hao, R. F. Tian, L. X. Zhang, L. Wang, *J. Phys. Chem. B* **2004**, *108*, 6311.
[30] Y. Q. Wang, C. J. Tang, Q. A. Deng, C. H. Liang, D. H. L. Ng, F. L. Kwong, H. Q. Wang, W. P. Cai, L. D. Zhang, G. Z. Wang, *Langmuir* **2010**, *26*, 14830.
[31] Y. Q. Wang, G. Z. Wang, H. Q. Wang, W. P. Cai, L. D. Zhang, *Chem. Commun.* **2008**, 6555.
[32] R. X. Xu, X. Y. Yu, C. Gao, Y. J. Jiang, D. D. Han, J. H. Liu, X. J. Huang, *Anal. Chim. Acta* **2013**, *790*, 31.
[33] W. Zhang, Y. B. Wang, Z. Wang, Z. Y. Zhong, R. Xu, *Chem. Commun.* **2010**, *46*, 7631.
[34] J. Pu, T. T. Wang, H. Y. Wang, Y. Tong, C. C. Lu, W. Kong, Z. H. Wang, *ChemPlusChem* **2014**, *79*, 577.
[35] Z. H. Zhu, J. Ping, X. P. Huang, J. G. Hu, Q. Y. Chen, X. B. Ji, C. E. Banks, *J. Mater. Sci.* **2012**, *47*, 503.
[36] L. Zhou, D. Y. Zhao, X. W. Lou, *Adv. Mater.* **2012**, *24*, 745.
[37] G. Q. Zhang, L. Yu, H. B. Wu, H. E. Hoster, X. W. Lou, *Adv. Mater.* **2012**, *24*, 4609.